# Fretting wear_Lubrication of initially worn parts through tribo-induced anchorage of PTFE in wear scars, and tribochemical creation of graphene oxide

Guillaume Colas[1,] *, Pierre-Henri Cornuault[3], Yann Michel[2], Romain Petre Bordenave[2]

[1] Université de Franche-Comté, CNRS, institut FEMTO-ST, F-25000 Besançon, France

[2] CNES, 18 avenue Edouard Belin, Toulouse, France

3 SUPMICROTECH, Université de Franche-Comté, CNRS, institut FEMTO-ST, F-25000 Besançon, France

*Corresponding author: guillaume.colas@femto-st.fr

**Keywords:** Fretting, wear, space, satellite, grease, alkyl-phosphonic acid, lubrication

## Abstract

Fretting wear during launch operation is a well-known cause of anomalies in spacecraft. In this study, a CubSat satellite stayed stuck in its dispenser during the final preflight qualification test. So close to launch date, not a single part of the satellite could be changed. A fretting test campaign has been carried out at laboratory scale to propose a solution to lubricate the damaged contacts. In depth expertise of the satellite allowed to determine the contact parameters. Damages and particles observed on the rail surfaces were successfully reproduced. The tests showed the appearance of a continuous flow of loose particles that either leave the contact or agglomerate inside it. Those agglomerating induced high friction and high adhesion. After contact opening and cleaning off the particles, lubrication was applied on the resulting damaged surfaces. Sprayed alkyl-phosphonic acid molecules and grease containing PTFE were selected to be tested as lubricant because they could be applied manually. PTFE accumulated in the damaged regions, protecting the surfaces from further damage while ensuring good lubrication. Sprayed alkyl-phosphonic acid molecules performed less. They however demonstrated in-situ tribochemical formation of a suspected graphene-oxide based lubricious 3rd body. Grease has been eventually chosen and the satellite successfully launched.

## 1 Introduction

Since the beginning of the space exploration, space tribology has been considered as an essential discipline to insure the success of space missions. Indeed, lubrication must be sustained not only in the vacuum of space, but also during operations on the ground, and this in different environments (simulated vacuum, dry and humid air, dry nitrogen). A space lubricant, fluid or solid, must therefore meet the challenge of providing the desired tribological behavior in these successive environments, but it must also resist the dynamic stresses induced by the launch. Although it is not mandatory for commercial satellite manufacturer to report the cause of anomalies, numbers of anomalies have been reported over the past decades [1]. A high proportion of those anomalies are related to tribology, launch loads, and release mechanisms [1–3].

To minimize the risk of failure, all mechanisms must pass numbers of qualification tests before being qualified for space flight. This means that all deployments, devices, motorizations and equipment have to be validated as working mechanisms to be sure they will function once in space. Even one-shot mechanisms, such as solar arrays and antennas deployment mechanisms, have to be tested multiple times [2–4]. Eventually, even the fully assembled satellite has to pass the tests to be qualified for spaceflight. Because of its size, the satellite itself cannot be fully tested in a vacuum chamber [5], i.e. during testing operations, its mechanisms and even onboard devices are exposed to clean room environments. Mechanisms are assembled on Earth, i.e. operators manipulate every piece that constitutes the device which is thus in contact with the surrounding environment. This operation is done in clean rooms whose humidity rate must be around or lower than (55±10)% at a temperature of 22°C±3°C [6]. Moreover, some mechanisms are stored for up to several years [7] in clean rooms. Another aspect to be taken into account is the transfer to the launch site [6].

During launch, the mechanism undergoes violent accelerations (up to several tens of g) and is subjected to noise (up to 150dB) and vibrations (lower than 10kHz) [4]. Indeed, besides natural vibration, the satellite is subjected to shocks [4,8,9] when the boosters ignite and when pyrotechnic detonations occur at every stage of rocket element separation. The frequency spectra of the vibrations is random in response to punctual events and noises [10]. Thus, for vibration testing operations on Earth, “envelope” functions are calculated to simulate the maximum/worst expected spectra depending on the mechanism and the launcher used [4]. Such vibrations are likely to result in the onset of fretting which is related to relative motions of contacting bodies with displacement amplitude much lower than the contact size [11]. Depending on the contact conditions (pressure, speed, displacement magnitude…etc) both fretting wear and/or fretting fatigue can occur, leading to a variety of surface modifications such as cracking, wear, oxidation, particles detachment, third bodies building-up, and even cold-welding [2,12–14]. As structural materials frequently employed in space applications, aluminum alloys were reported to be strongly subjected to fretting wear [13,15,16] even in the case of treated surfaces and/or grease lubrication [2,13,17,18]. Fretting damages are also discussed in the literature depending on the environmental conditions during the tests [12], and a specific procedure has been recently designed to study cold welding over a full launch sequence [2].

The present study deals with a fully assembled CubSat that did not pass the very last vibration tests to be qualified for space flight. The root cause of the anomaly has been found to be related to tribology. Based on the expertise of the damaged surfaces and the data from the qualification test, a fretting test campaign has been designed and conducted at the tribometer scale. The wear mechanisms have been studied and a solution has been found to eventually lubricate the damaged contacts.

## 2 Description of the anomaly

Figure 1 presents a picture of the CubSat and the dispenser in which it is stored and maintained in place during launch. Once in space, the satellite is ejected from it to then reach its orbit. The CubSat is rigidly held in place along the x axis. Along the y axis the satellite is hence hold by what could be assimilated to two elastic preloads. The preload is applied by a mechanical system on each of the CubSat lateral faces. Along the z axis, it is subjected to gravity only, and is supported on the lower face in the dispenser. Consequently, it might be subjected to shocks along the z axis if the satellite undergoes violent vibrations and displacements along this axis. The maximum clearance between the satellite and the dispenser guiding rails is 0.2mm (+/-0.1mm).

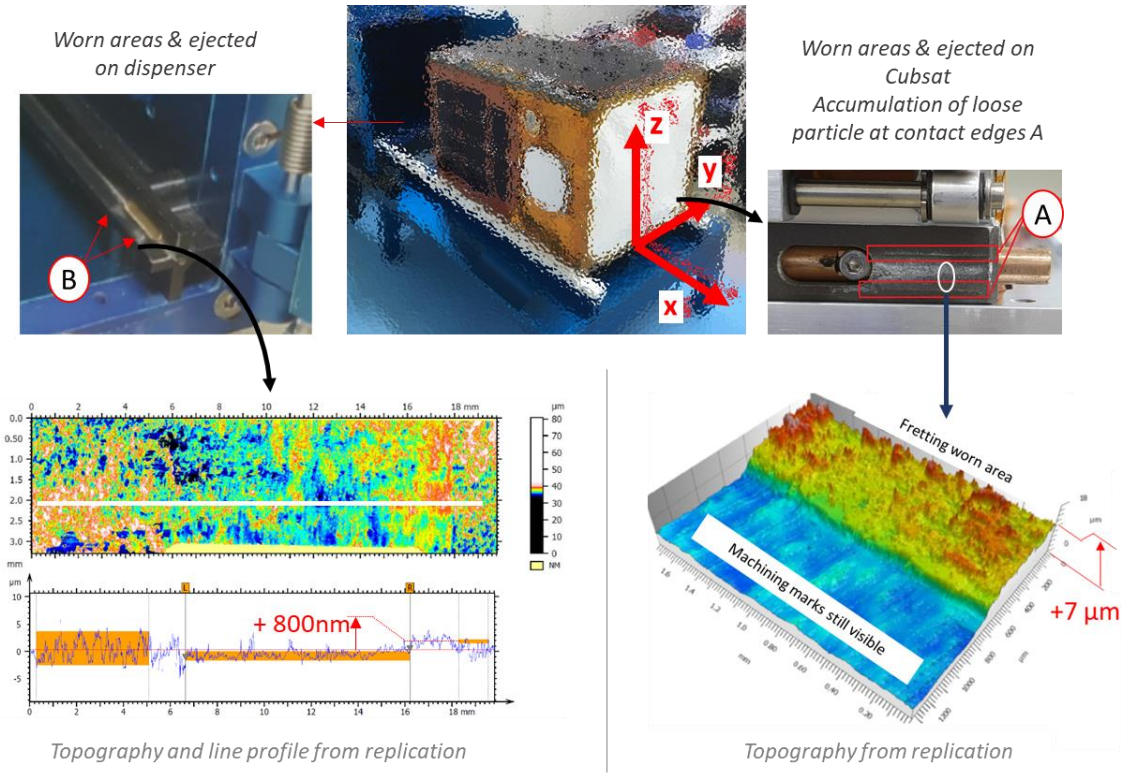


*Figure 1 - Magnification of the worn areas of the dispenser and the CubSat. The image is intentionally not scaled. The topography of the surfaces is obtained from surface replication, which means that height increase refers to material removal and consequently refers to wear. Replication are done on cleaned surfaces, i.e. after removal of the particles*

To be fully qualified for space flight, it has to be ejected outside the dispenser right after a sequence of vibration test emulating the launch. In the present case, the CubSat stayed stuck inside the dispenser. It had to be taken out of the dispenser manually. The study of the vibration data showed that the main eigenmode observed during the satellite vibration tests in the dispenser lies between 60 and 100Hz. Given the collapse of the eigenmode observed during the satellite tests, it is likely that there is contact between the lateral faces of the satellite with the dispenser. It is not possible to determine the amplitude of the deflection by analysis of the vibration behavior due to the lack of instrumentation. Given the manufacturing and assembly tolerances, it is believed that the realistic clearance is likely to be in the range of 0.1mm.

Inspection of the surfaces demonstrates the presence of wear debris in and around damaged areas on guiding rails on both the dispenser and the CubSat (Figure 1). Wear is localized in specific regions closed to rails extremities. The damaged areas were about 440mm². Assuming that the contact between the satellite rail and the dispenser guiding rail is perfect flat-on-flat contact, considering the preloads, and the area of the damaged areas, the lowest possible contact pressure would be around 1.8 MPa. The morphologies and traces observed on the satellite (insets on Figure 1) most likely indicate friction along the y axis, i.e. along the preloaded axis. That is evidenced by the ejection of wear particles along both the dispenser and the satellite rails (regions A and B). There is no evidence of impact resulting from movements along the z axis, this cannot however be excluded considering wear appeared significant (significant amount of debris).

To better localize wear and its origin, the topography of the surfaces has been studied in terms of roughness variation and depth of wear. On satellite side, wear depth of ~7 µm has been measured while almost no wear has been detected on dispenser parts (~800 nm). In the latter case, it appears

that the surface has been smoothed. EDS analysis showed that wear particles appear mostly comprised of aluminum oxide. Fluorine (F) has also been slightly detected, which appears to corroborate the presence of some PTFE that most likely originates from the Hart-coat Plus © surface treatment of the dispenser rail (Table 1). However, the surface treatment of the satellite rails (Surtec 650) has also been shown to contain F [19]. Attention will hence be given to the composition of the materials and surface in the laboratory scale study to fully determine the origin of wear.

# 3 Materials and methods

## 3.1 Materials:

Materials of interest are the materials constituting the dispenser guiding rails and CubSat rails (Table 1). The CubSat is made of aluminum 7075 with hard anodizing surface treatment and coated with Surtec 650 coating. Surtec 650 has been presented has replacement to hexavalent Cr containing coating [20]. It has also been recommended for use on 7075 aluminum alloy [20]. Guiding rails from the dispenser are made of aluminum 7021 treated with Hart-coat Plus © (harcoat treatment with addition of PTFE).

*Table 1 - material composition*

| | Dispenser | CubSat |
|---|---|---|
| Substrate | Al_7021 | Al_7075 |
| Surface treatment | Hart-Coat Plus ©: hard anodizing + PTFE | Hard anodizing + Surtec 650 |

The lubricants to be tested must be applicable easily, quickly, directly on the CubSat rails without disassembling any part, nor risking to requalify any equipment. This means that they have to be applied on the damaged parts. The only qualification test that had to be passed is the ejection test following the vibration tests emulating launch (vibrations, noise, shocks). The selected lubricants are the following:

- ➔ Grease MAPLub ® PF 100-b, it is a PerFluoroPolyEther (PFPE) based grease with PolyTetraFluoroEthylène (PTFE) particles dispersed in it. The application is done manually by directly applying grease on the parts.
- ➔ Alkyl-phosphonic acid molecules dispersed in alcohol solutions. This solution is sprayed directly on the surface, and then it left to dry. During the evaporation of the solvent, the molecules create a self-assembled molecular layer on the surface.

## 3.2 Fretting tests:

The targeted contact is a plane on plane configuration, although it is rather difficult to obtain. The rationale driving such a choice is to be as close as possible to the real situation, and to recreate the morphologies of both the wear marks and the particles. There was no evidence leading to univocally assert a plane on plane contact on the real contact, particularly considering the localization of the worn areas and the parts. Finally, a point contact, such as a ball on plate configuration, may directly hinder particle circulation and trapping between the surfaces in contact, which would not be representative

of the real case. To optimize the sample mounting, samples were put in contact, and only then all screws were tightened. The tilt between the surfaces is hence limited, which in turns limits the opening of the contact. Marks were also added on the holder of cylinder sample to mount the cylinder always in the same position. After analysis of the surfaces of the unlubricated test, the damaged areas (used to calculate height distributions, see section 4) are, over the 3 tests: 15.6 ±0.5 mm² on the cube and 10.9 ±0.8 mm² on the cylinder. Regarding the samples from the lubricated tests, they were not dismounted from the tribometer. However, visual inspection of the samples prior application of the lubricant demonstrated that it remains similar over the all tests.

The samples emulating both the dispenser's guiding rail and the CubeSat rail counterpart are manufactured following exactly the same manufacturing process than the real parts. The sample emulating the dispenser is a parallelepiped. The height x width x length dimensions are 12mm x 14mm x 14mm (Figure 2). The parallelepiped is called cube in the following. The sample emulating the CubeSat rail is a cylinder of 8mm in diameter and 20mm in length. Chamfer at the edges makes diameter of the end disc of the cylinders equals to 7mm (Figure 2).

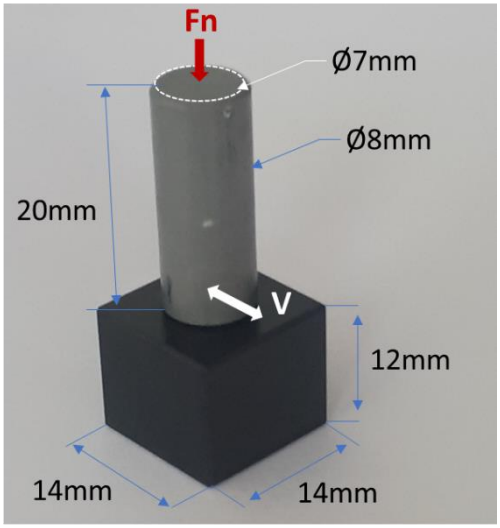


*Figure 2 - Samples dimensions and positions relative to one another. Load is applied from above and the cylinder is the moving sample.*

In order to find the contact conditions able to reproduce the wear behavior of the contact, set of parameters has been defined and tested. The baseline was set on the lowest possible contact pressure estimated from the expertise of the satellite (1.8 MPa), and assuming a perfectly flat on flat contact. Due to the dimensions of our cylinder sample, and assuming perfectly flat on flat contact, the normal load is estimated to be 70N. The flat on flat assumption cannot be valid because wear is localized on specific areas on both the CubSat's rails and the dispenser's guiding rails. Consequently, it is underestimated. Moreover, the estimation from the satellite does not consider the amplitude of displacement, the accumulation of debris, and localization of wear within the contact. The real load bearing bodies (thick patches of agglomerated debris) and/or surface could be fewfold lower than the baseline estimation. Consequently, the contact pressure could be fewfold higher. The tribometer used for the tests is the Plint TE77 tribometer, which limits the oscillating frequency to maximum 50Hz in this study. However, the tribometer eigenmode has been excited during the tests performed in the range of 40Hz to 50Hz. Frequencies higher than 40Hz were hence excluded. The qualification tests data showed that it is not expected to have major behavioral transitions between 40Hz and 100Hz.

Nonetheless, if the sliding speed has major contribution to the anomaly, a range of amplitude has to be considered. On the CubSat, if the sliding occurs over the over the maximum clearance range and at 100Hz, the maximum sliding speed would be 40 mm/s.

The list of the parameters to be tested and their values is the following:

- Reciprocating within a different full amplitude: 75µm, 160µm, 300µm, 600µm
- Load: 70N, 140N, 270N
- Frequency: 5Hz, 30Hz, 35Hz, 40Hz
- Test duration: 3min, 8min, 32min, 68min

All tests are performed in laboratory air at a relative humidity of 43±4 %HR, and at a temperature of 22±1 °C. Friction forces are measured by a Kistler piezoelectric sensor, normal load is continuously monitored by gauge sensors, and displacement is continuously measured by non-contact optical sensor. Sampling rate is set to 5 kHz for the tests conducted with reciprocating frequency of 30 Hz and above, and to 1 kHz for the tests conducted with reciprocating frequency of 5 Hz.

Eventually, the final set of contact conditions that are preproducing both the wear behavior observed on the CubeSat (in terms of the surface morphology of the worn area, the particles generated, and ejected) is: reciprocating full amplitude of 600µm, normal load of 140N, frequency of 30Hz (equivalent to 36 mm/s sliding motion), and test duration of 3 min. A summary of the results leading to this choice can be found in supplementary material (SM_#1). Figure 3 displays pictures of the cube and cylinder samples after fretting test in the selected contact conditions. As expected, only a portion of the surfaces are really in contact and worn. The morphologies are nonetheless optically similar to what is observed on the real parts. Further investigations are presented in the following sections.

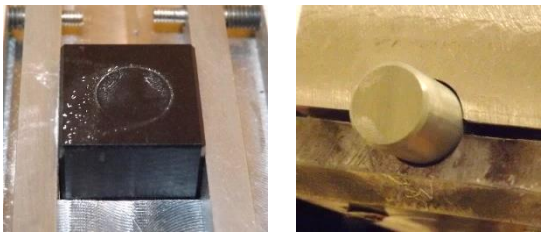

(a) (b)

*Figure 3 - Samples surfaces after test in the optimal configuration (600 µm full amplitude, 30Hz, 140N); (a) the cube sample emulating the dispenser guiding rail; (b) the cylinder emulating the CubSat rail*

Adhesion between the parts appeared to be of great importance and might be a stronger contributor to the anomaly than a high friction coefficient. Adhesion must consequently be considered into the laboratory scale fretting tests and analysis. The satellite is ejected along the x axis which is orthogonal to the most likely sliding directions (y axis) during vibration, while it remains under normal loading along z axis. It has nonetheless been decided to restart a test at low frequency (5Hz) during only 2 seconds, with 1kHz sampling rate, after the 30Hz fretting tests. The purpose is to tentatively assess if a maximum shear force is required to induce sliding at the interface. Moreover, during the fretting test at 30Hz, a “tac-tac-tac” periodic sound is heard and let one think that it might be related to the formation and rupture of adhesive bounds between the two counterparts at each cycle (cf. Video#V1 supplementary material). Only then the contact is unloaded and finally opened with a dynamometer to access to a possible remaining adhesion force at the contact. Figure 4 presents the diagram of the test sequence.

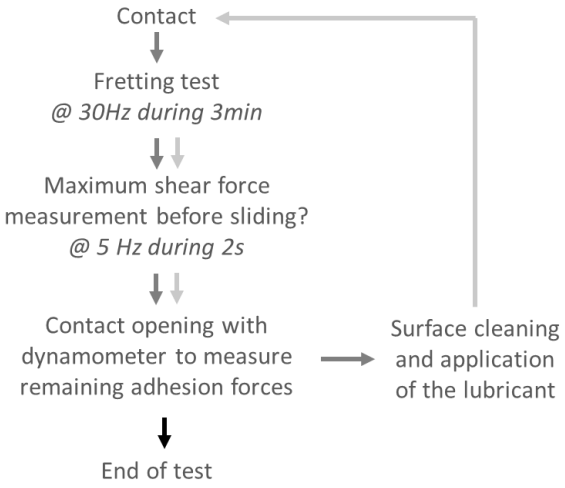


*Figure 4 - Friction test rationale demonstrating the exact repetition of the fretting test sequence between unlubricated (dark grey arrows) and lubricated (light grey arrows) test that follows the unlubricated one, and using the same samples.*

Figure 4 also shows that both the surfaces are cleaned prior the application of the lubricants. Cleaning is performed using clean room rated wipes and isopropyl alcohol. Note that lubricants are applied on parts that had previously underwent dry sliding fretting test. This choice is driven by the Cubesat situation, lubricants will indeed be applied on the worn parts of the satellite itself. At this stage of qualification, not a single part can be changed. lubricants are applied on the worn surfaces of the sample emulating the Cubsat rail (i.e. the cylinder) after it is cleaned. Then the contact is closed again, and the test sequence with the lubricant remains the same. The grease lubricant is applied manually by putting a small amount of grease on the index finger, which is then pressed onto the worn surface of the cylinder previously cleaned (SM_#4 presents pictures of the lubricated surface). The alkyl-phosphonic acid molecules are sprayed on the surface. To do so the spray is positioned 5 cm away from the cylinder surface and 3 brief spray are performed. Then the surface is left 4 min exposed to laboratory air to let the solvent evaporate and let the molecules organizing themselves. It is worth mentioning that such procedure leads to the chemisorption of the molecules on the substrate and to the physisorption of molecules aggregates onto the chemisorbed layer [21].

## 3.3 Post-test Analysis

Pristine and worn surfaces' morphologies are analyzed using both optical and electronic microscopy techniques. 3D topographic images of the surfaces are obtained using Alicona Infinite Focus microscope. The topographic data is then processed using Gwyddion to study the thicknesses of 3$^{rd}$ body materials, and the depth of worn region. FEI Quanta 400 Scanning Electron Microscope (SEM) is then used to study the morphologies worn surfaces into more details, and to obtain information on the local distribution of the 3$^{rd}$ body materials. The low-pressure imaging mode is used because the surface treatment of the samples is an insulator, and the surface modifications induced by the electron beam was too important in the regular vacuum imaging mode. Energy Dispersive X-Ray Spectroscopy (EDS) was conducted in combination with SEM imaging to study the elemental composition of the worn surfaces and 3$^{rd}$ bodies. Composition was, hence, associated with the 3$^{rd}$ body distribution and morphology. SEM imaging and EDS analysis are performed at 20 keV.

Fourier Transform InfraRed spectroscopy (FTIR) analyses have also been performed, but only on samples that underwent lubricated test. The FTIR measurement have been performed on an 8700-Nicolet spectrometer in Attenuated Total Reflectance (ATR) mode using a ZnSe internal reflectance element (IRE). Transmittance was measured in the mid-infrared region (800 – 4000 $cm^{-1}$) with a 2 $cm^{-1}$ resolution, and the IRE was gently cleaned with ethanol between each analysis. Background analysis was also performed to remove the contribution of the surrounding environment to the measures.

# 4 Results and Discussion

## 4.1 Friction coefficient

Figure 5 shows the fretting loops obtained during the initial unlubricated configuration emulating the anomaly. Friction forces are presented in terms of the variations of their amplitude over one cycle along the track length (1st and last cycle), and over the whole test as a 3D plot. Results from the 5Hz experiments are also given. The presented friction variations are representatives of what has been observed for all tests performed. The high reproducibility of friction behavior is clearly seen with the unlubricated configuration, presented twice in SM_#5 for the two different tests.

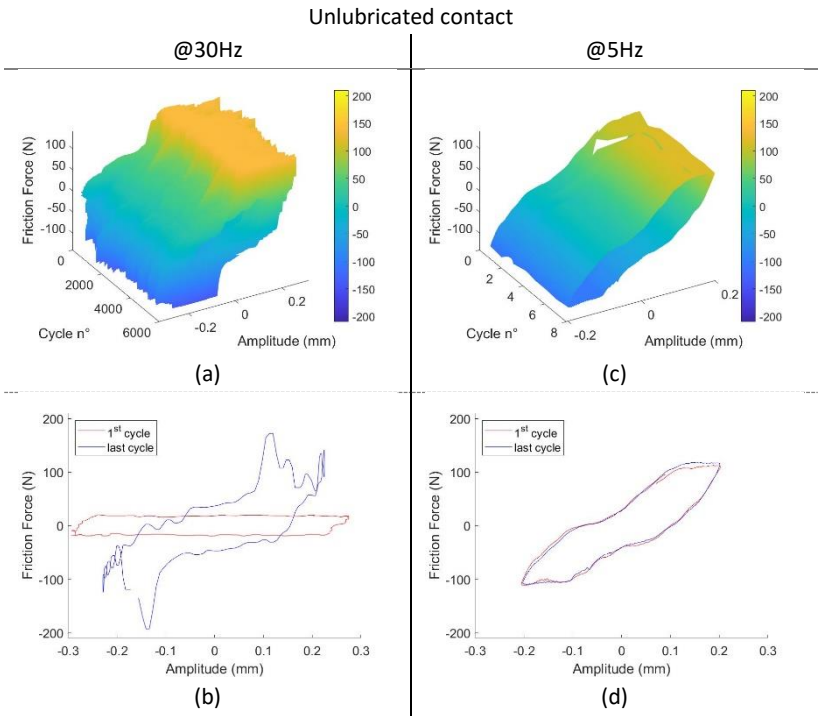


*Figure 5 – Fretting Friction force loop of unlubricated test. (b) and (c) are the 2D representations of the first and last fretting loops of the 3D plots (a) and (b) respectively*

The fretting loop (narrow and inclined loop shape), which is a direct evidence of adhesive contact in fretting with partial slip, is clearly observable. The partial slip regime has been shown not to be sensitive to humidity in the torsional fretting wear of 7075 aluminum alloy [12]. Moreover, Zhang [22] did not discuss any dispersion in the fretting behavior of the same alloy while working in a range of humidity lying between 40%HR and 55%HR, and at 22°C. The possible impact of lower relative humidity of the laboratory tests, as compared to the clean room environment in which the qualification tests are conducted, may hence be minimized in the study. Sliding occurs only over a short distance of ~150 µm with a very high mean friction force (~100N, i.e. ~0.7 friction coefficient). Before sliding

starts, a high static friction force of ~180N (~1.3 friction coefficient) is noticeable, which demonstrates significantly high adhesion. It is believed that this is also the reason for the "*tac-tac-tac noise*" heard during the test (cf. video#1 in supplementary materials), and which fully covers the motor noise that can be heard during lubricated tests (cf. video#2 in supplementary materials). The first cycle, during which sliding only occurs on surfaces oxides and contaminants is almost rectangular, demonstrating sliding over most of the oscillation amplitude (Figure 5b). Sliding friction during the first few cycles remains low around 0.1. Then the friction rises quickly and the friction loop narrows significantly. The quick transition to fretting loop demonstrates the creation of adhesive bounds within the contact. The transition also corresponds to the moment when particles start to be ejected outside the contact as it can be observed on the video *Video#1* (supplementary material). A continuous ejection of white particles can indeed be observed.

Fretting loops obtained at 5Hz oscillation frequency (Figure 5d & c) demonstrate the absence of very high static friction force. They also show that sliding occurs over 100µm and is very smooth. Nonetheless, the friction remains high and equals ~100N (~0.7 friction coefficient) during sliding. The overall shape of the loop is very similar to the last fretting loop obtained during the fretting test at 30Hz oscillation frequency (Figure 5b). That means the interface remains stable and the tribological response of the damaged surface is not impacted by the sliding speed within the range of oscillating frequency considered. At the contact opening loose particles can be seen, as well as a dense white 3$^{rd}$ body layer located where the contact took place. Although it appears bounded to the substrate, manual gentle cleaning of the surface with wipes and isopropyl alcohol is sufficient to visually remove all the white 3$^{rd}$ body.

Once the contact is cleaned and the lubricant is applied on the damaged surface of the cylinder, the friction response of the contact lubricated with MAPLub ® PF 100-b grease is very stable (cf. Figure 6). Fretting loops are consistent with pure sliding lubricated contact. Sliding occurs over the full desired displacement range. Friction coefficient remains around 0.1 (friction force around 15N) all along the test. Similarly to what is observed in the unlubricated case, the first cycle exhibits less variations than the last one (cf. SM_#5), however the friction force is not increasing and the low friction is maintained. Subsequent test at 5 Hz oscillating frequency shows very stable friction with the same friction force (Figure 6 and SM_#5). The contact lubricated with alkyl-phosphonic acid molecules also demonstrates low friction force around 15N (Figure 6). It however increases locally leading to a friction force that can reach ~40N (0.3 friction coefficient) in the middle of the friction track with a local pic around 140N similarly to the unlubricated case. The fretting behavior has transitioned from full slip to a fretting mixed regime with sliding happening over ~300µm. The subsequent test at 5Hz (Figure 6) is similar to the unlubricated fretting test, the fretting loop is however approaching a parallelogram with a sliding distance in the range of 200 µm to 250 µM, and a friction force of 100N (0.7 friction coefficient). The fretting regime is hence closer to a mixed regime.

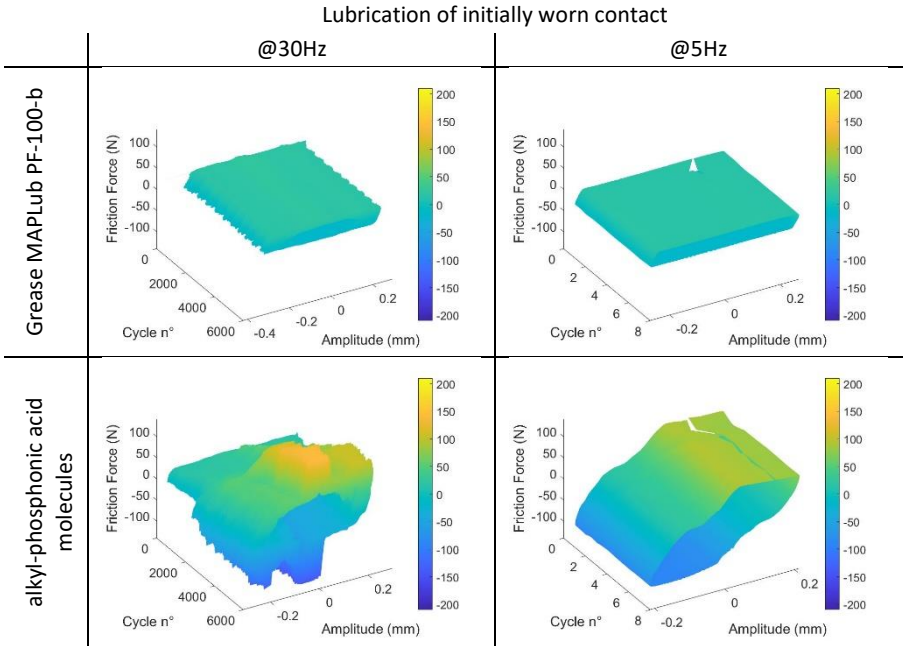


*Figure 6 - Fretting friction force loop of the lubricated test. Lubricant is applied on the initially worn part obtained for the fretting in dry sliding condition*

In terms of particles ejection, no particles are ejected during the lubricated tests at both 30 Hz and 5 Hz oscillating frequencies with the MAPLub ® PF 100-b grease. The surface is not damaged visually and areas initially worn appear smooth and homogeneous. A halo of grease is observed on the cube around the contact (cf. SM_#2). The contact lubricated with the alkyl-phosphonic acid molecules exhibits ejection of few particles starting approximately after 3,000 cycles of sliding. This corresponds to the start of the increase in friction coefficient locally. Particles ejection, although limited, appears to demonstrate the onset of a lubrication failure similar to what is observed during the fretting unlubricated tests. This is consistent with the shape of the friction loop obtained during the 5 Hz test as discussed above. Pictures of the samples lubricated with the alkyl-phosphonic acid molecules can be found in SM_#6.

The remaining force of interest in the study is the force required to open the contact after contact unloading. Note that during unloading the contact after unlubricated and alkyl-phosphonic acid molecules lubricated tests, a brief loud and sharp sound is heard and attributed to the breaking of adhesive bounds at the interface. The opening force after unlubricated fretting test is 10.3±2.3 N. After lubricated fretting tests with the MAPLub ® PF 100-b grease the opening force decreases to 8.5±1.3 N, and falls to ~7N (only two measures) when the contact is lubricated by alkyl-phosphonic acid molecules. It is surprising that the alkyl-phosphonic acid molecules offer the lowest remaining adhesion at the contact opening considering the onset of lubrication failure, and the fretting loop observed during the tests at 5 Hz. It is believed that adhesive bounds are created in areas that are not lubricated anymore. Then, the unloading breaks those bounds, and the 3$^{rd}$ body that eventually remains inside the contact is sufficient to separate both parts under low load. Contacts between worn regions are thus prevented.

## 4.2 Post-test friction track analysis of unlubricated contact

In order to perform surface analyses of the samples and reveal the surface and 3$^{rd}$ bodies morphologies, unlubricated samples have been analyzed without cleaning them. Figure 7 shows a

topographic study of both the cube and the cylinder samples after an unlubricated fretting test. In this case, only one primarily load carrying region is observed. This region is characterized by a thick 3rd body layer on the cube sample. The height distribution reveals that the thickness is as high as 14µm above the pristine surface of the substrate. The asymmetric height distribution of the 3rd body reveals that the layer surface is rather made of valleys and a "flat" top surface. On the cylinder, the worn region can be divided into two regions: a worn region located at the edge of the sample and one region closer to the center of the cylinder. The worn region exhibits a wear depth of about 4 µm, while the second region sees its height distribution centered on zero. This second region however exhibits a narrower height distribution than the one obtained on pristine material. Moreover, machining marks are not visible anymore on the cylinder surface after the fretting test, which means that the surface has been "polished" by friction. Considering the Gaussian nature of the distribution, it can be assumed that the tribology induced surface modification is not limited to removing pics. The resulting surface is indeed very different from the cylinder pristine surface. Optically it also appears very dark as compared to the pristine surface.

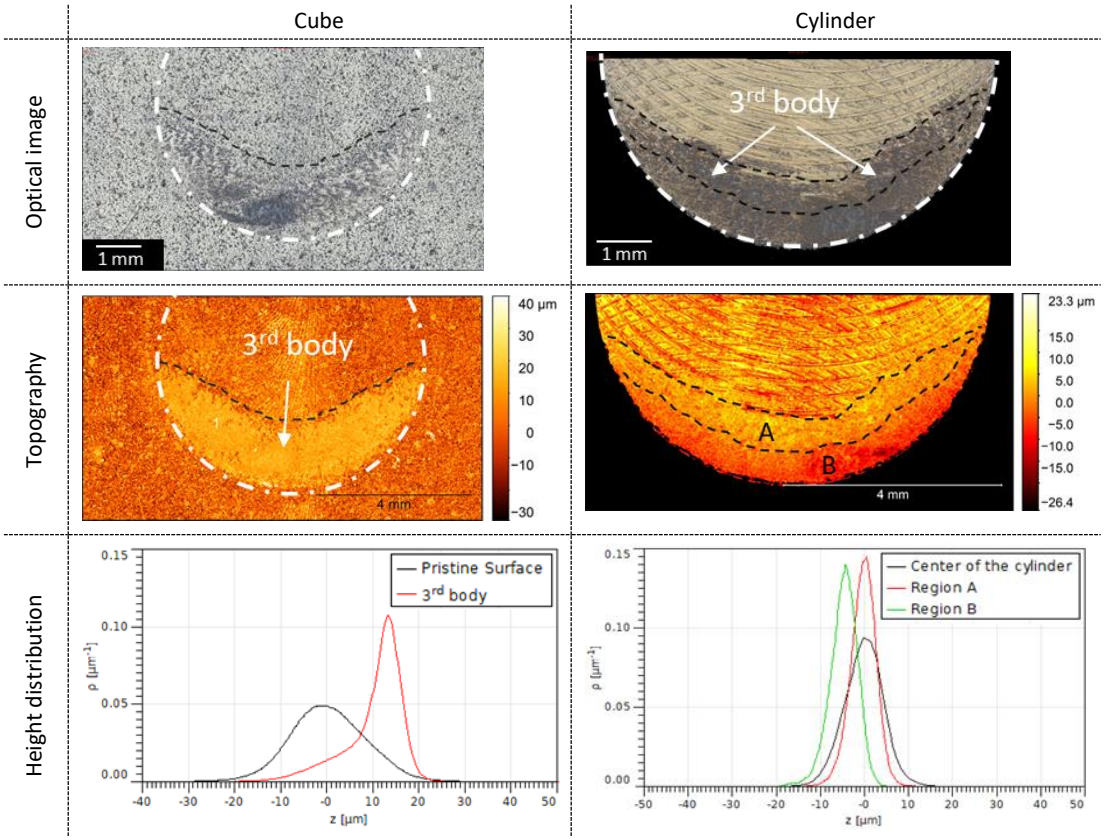


*Figure 7 - Thickness of 3rd body inside the friction track on both the cylinder and the cube samples.*

The SEM analysis of both the pristine and of the worn surfaces of the cube (Figure 8a) shows that the 3rd body is composed of particles heavily compacted into a thick layer around which lies less compacted 3rd body. The surface features, particularly the periodic ones, observed on top of the layer are typical of adhesive contact. Few loose and volatile 3rd body particles/debris are observed inside the contact. However, most debris are observed outside this region, which is consistent with the continuous ejection of particles during the unlubricated fretting tests. Consequently, the denser 3rd body most likely carries all the load. EDS analysis (Figure 8b) shows that the composition of the 3rd body is a combination of both the cube and cylinder materials. The neat increase in Zr, and Cr detections is an evidence of the presence of material coming from the cylinder (Figure 9, EDS analysis). The oxygen content is however significantly higher than what it is detected on the pristine materials,

which is typical of tribo-oxidation seen during fretting tests in air [2,12]. Carbone is also detected in the 3rd body, but it is not detected in pristine material. Fluorine is detected in the 3rd body but not in the pristine material. This is surprising considering that the cube surface is supposed to be coated with PTFE. It is believed that the PTFE layer is very thin and that the contribution of the bulk material to the EDS analysis is hiding it. Considering the cube is not significantly worn, contrary to the cylinder, F detection in the 3rd body is attributed to the debris coming from the latter. The Surtec 650 has indeed been shown to contain F in its composition [19].

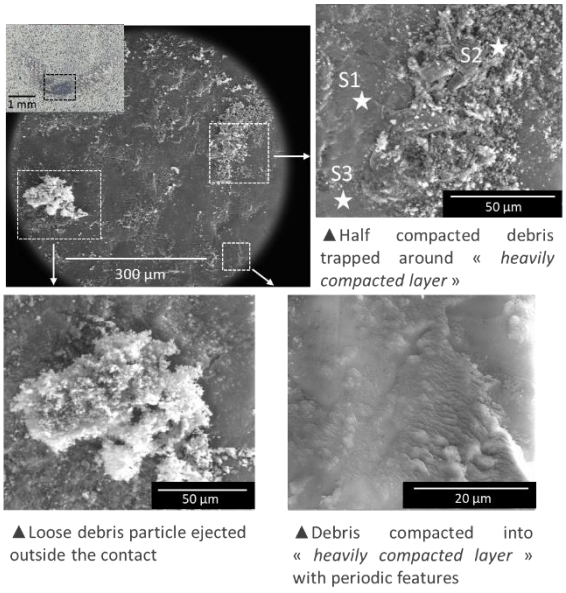


(a)

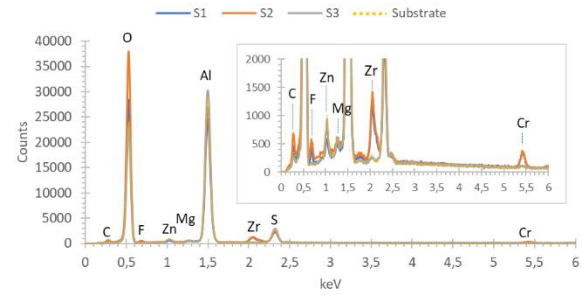


(b)

*Figure 8 – (a) SEM observation of the cube sample after fretting test without lubrication; (b) EDS spectra measured in locations S1, S2, S3, and a spectrum obtained on pristine cube surface*

To the contrary, the 3rd body on the cylinder exhibits a composition that is only relevant to the cylinder composition itself (Figure 9b). That means the 3rd body material most likely originates from the cylinder. Such observation is consistent with what is observed on the CubSat. Moreover, the worn region at the edge of the cylinder (Figure 9a, first row images) where material is removed demonstrates that the oxide layer is significantly damaged. Its fibril porous microstructure is indeed exposed. In the second region (Figure 9a, 2nd row images), the SEM images show that plates of 3rd body is sitting on top of the machining stripes. The loose particles are trapped and compacted around them and in the grooves, which eventually results in a smooth surface morphology and the narrow height distribution (Figure 7).

All the observations described here for a surface with only one worn region remains relevant for samples exhibiting two worn regions on the sample surfaces (cf. SM_#3).

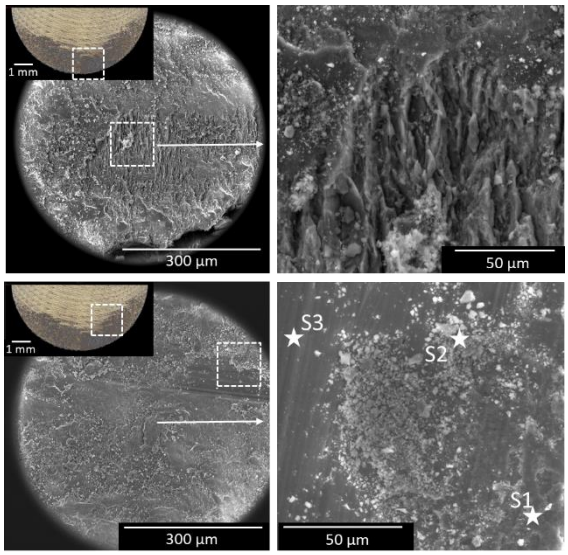


(a)

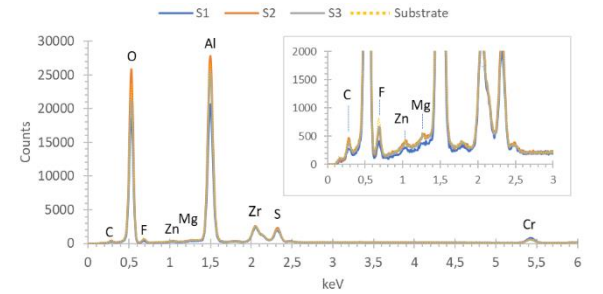


(b)

*Figure 9 – (a) SEM observation of the cylinder sample after fretting test without lubrication; (b) EDS spectra measured in locations S1, S2, S3, and a spectrum obtained on pristine cylinder surface*

## 4.3 Post-test friction track analysis of lubricated contact

The surfaces of the samples that underwent the grease lubricated fretting test were gently cleaned using isopropyl alcohol to remove the excess of grease, while keeping as much 3rd body as possible on the surfaces. The samples lubricated with alkyl-phosphonic acid molecules were analyzed as is because the solvent has been evaporated before the test started, which resulted in a dry friction configuration.

Regarding the grease lubricated case, the topographic analysis (Figure 10) demonstrates the high propency of the grease to bound to the cube surface. The height disribution indeed reveals that the thickness of the remaining materials in the “ring of grease” region is close to 9µm, which lies between the height of the lightly loaded center region of the contact (8 µm thick), and the initial worn region which concentrates a thick 3rd body whose thickness is 10 µm. On the cylinder sample, similar observation is made. Initially worn surfaces concentrate 3rd body whose thickness is around 4 µm above the lightly loaded center region of the contact surface. Note that the height distribution of the center region remains the same than in the case of unlubricated fretting test during which the center region has not been damaged. Such observation thus implies that the MAPLub ® PF 100-b grease is less prompt to bound to the cylinder surface as compared to the cube sample.

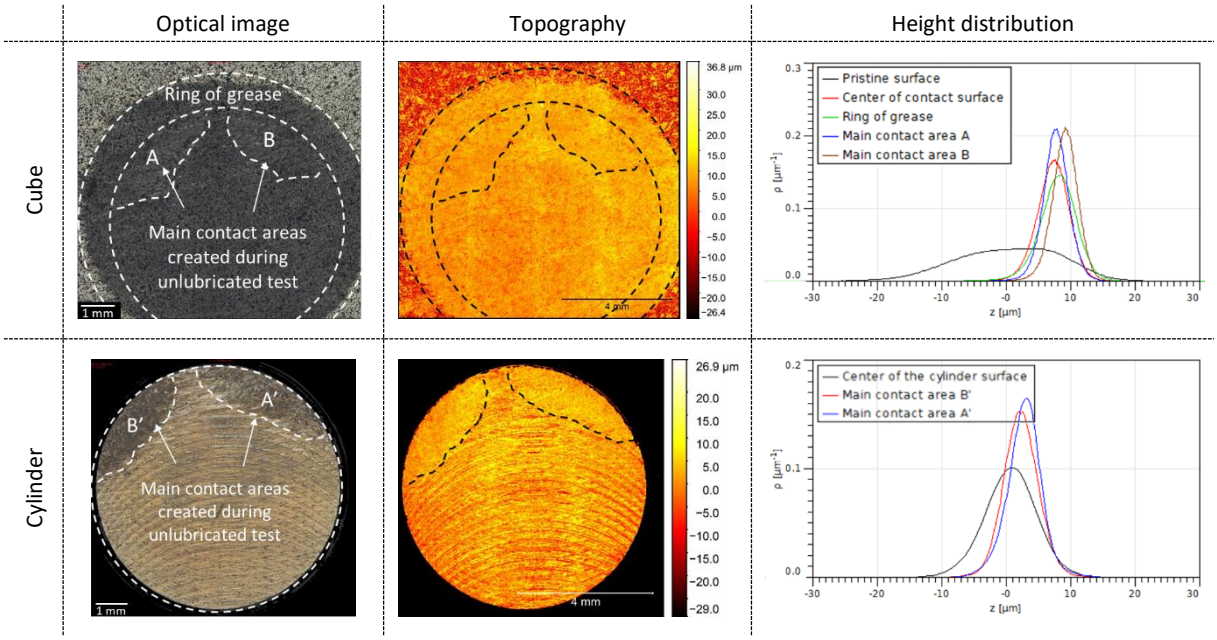


*Figure 10 - Thickness of 3rd body inside the friction track on both the cylinder and the cube samples after lubricated tests with MAPLub ® PF 100-b grease*

The SEM images of the cube surface (Figure 11a) reveals the presence of a rather homogeneous and continuous layer of 3rd body in the worn region. Similar but thinner 3rd body is observed in the center region of the contact (area B). The EDS analysis reveals the detection of F in the elemental composition of the 3rd body. The detection of Zr in the EDS spectrum obtained inside the main contact areas (area A) created during unlubricated tests shows the presence of remnants of 3rd body from the cylinder. Nonetheless, based on the surface morphologies, a 3rd body layer covering the surface after lubricated test is similar to the one covering the initially unworn region. Complementary ATR-FTIR analyses (Figure 11c) reveal that the 3rd body detected is essentially comprised of PTFE based material. This is consistent with the grease composition which contains PTFE particles dispersed in it. The detection of PTFE as a smooth, thin, and quasi-continuous layer indicates that PTFE actively takes parts in the lubrication. No particles are observed both inside and outside the contact. The cylinder exhibits a similar 3rd body layer in the initially damaged areas (Figure 12). There is however no clear evidence of 3rd body layer inside the lightly loaded region (center region of the cylinder contact surface). Finally, FTIR analysis (Figure 11c) shows a low detection of PTFE as compared to the cube. That means that the PTFE and the grease are not naturally bounding to the cylinder surface.

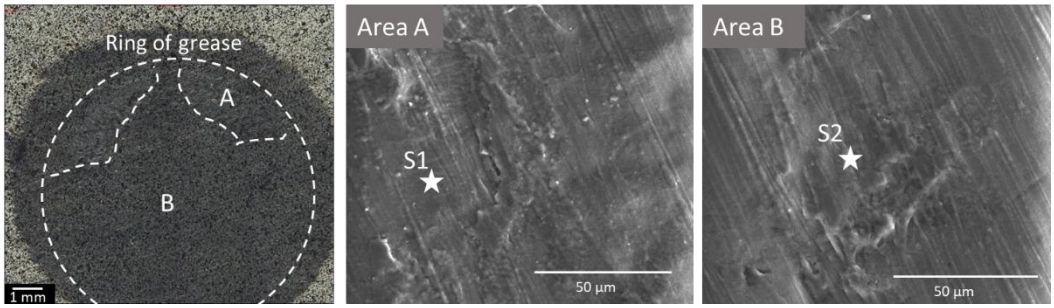


(a)

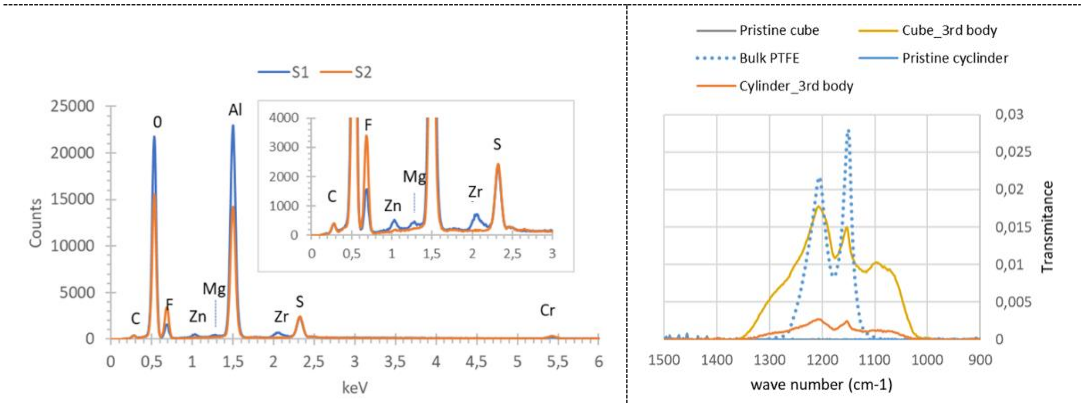


(b) (c)

*Figure 11 – SEM (a) and EDS (b) analyses of the cube surface after lubricated test with MAPLub ® PF 100-b grease; (c) FTIR spectrum of the 3rd body created during the grease lubricated test on both the cube and cylinder surfaces*

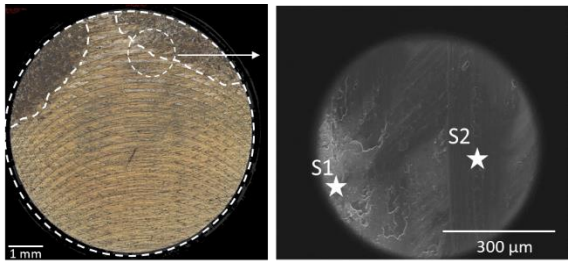


(a)

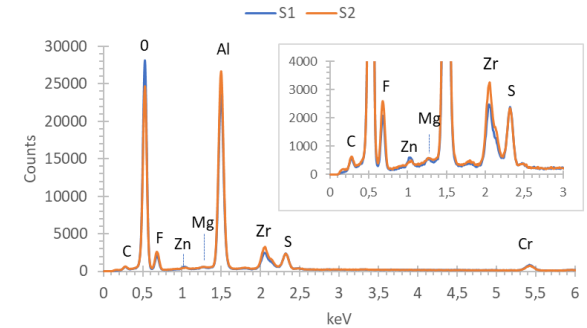


(b)

*Figure 12 - SEM (a) and EDS (b) analyses of cylinder surface after lubricated test with MAPLub ® PF 100-b grease*

The alkyl-phosphonic acid molecules exhibit a different response to friction. The surface of both the cylinder and the cube visually appear significantly covered by 3rd body originating from the lubricant (Figure 13). Two types of 3rd bodies are observed: one that is demonstrating whitish color at naked

eye, and one that is very dark, almost black. On both the cube and the cylinder, the dark 3rd body is very thick, around 8 µm above the mean surface of the pristine material. Note that "pristine" term used for the cylinder is to describe the visually unworn surface is debatable considering the height distribution of the region is not gaussian but rather a bimodal function (Figure 13). Top asperities may have been removed, which might result into a plateau and valley morphology. Note that the maximum of the height distribution of the dark 3rd body on the cylinder is at the same position than the 2nd maximum of the height distribution of the "pristine like surface". That means the dark 3rd body fills the valley and thinly covers the top surface of the plateaus. On the cube, the white 3rd body is thinner than the dark one. It however has a thickness of 5µm, which is close to the mean value of the overall friction track thickness (~6µm). On the cylinder, the white region corresponds to a heavily damaged region. A significant amount of the material has been worn out. The white region is indeed 10µm deep in average.

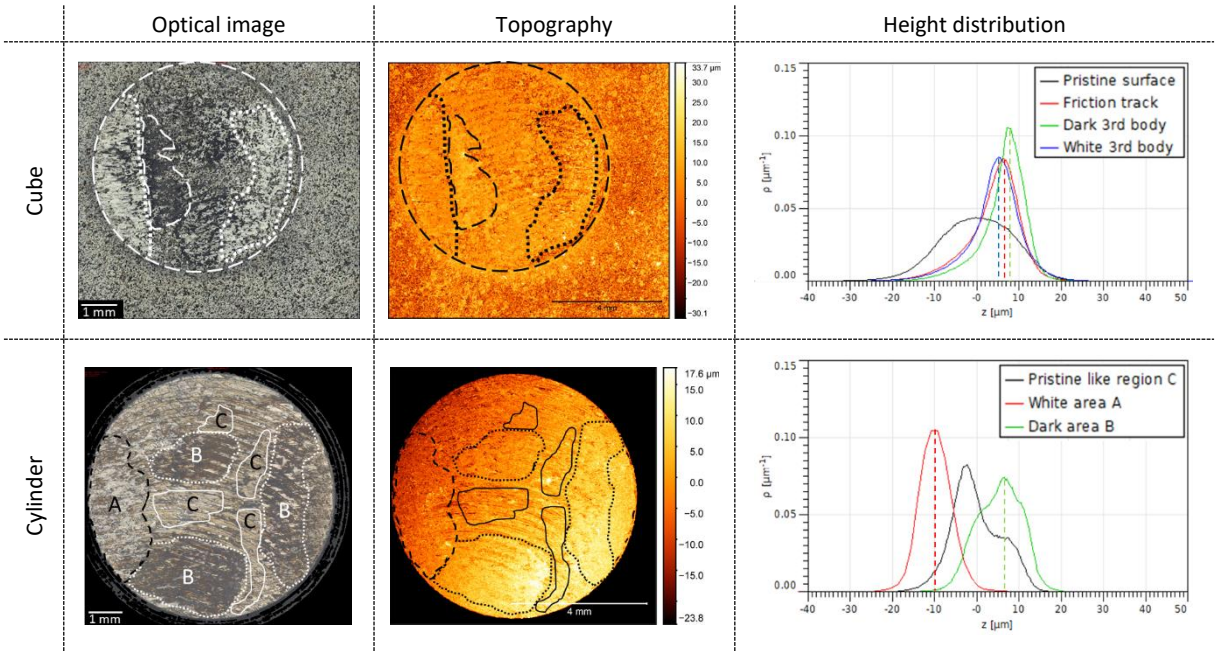


*Figure 13 - Thickness of 3rd body inside the friction track on both the cylinder and the cube samples after lubricated tests with alkyl-phosphonic acid molecules*

The SEM and EDS analyses (Figure 14) shows that the 3rd body exhibits two different morphologies and compositions. One is granular and one is rather dense. Interestingly, elemental compositions appear slightly different. In the composition of the dense 3rd body, neither F nor Zr are detected on S2, but P is detected. That demonstrates that the dense 3rd body is essentially comprised of materials originating from the alkyl-phosphonic acid molecules. The alkyl-phosphonic acid molecules tested here are indeed composed of an anchorage group containing P, and a long C based chain. They are known to bound well with hydroxyl groups and metal oxides [23]. Through solution spraying and subsequent solvent evaporation, it is known that a significant amount of molecules anchor to the substrate to create a thin chemisorbed layer while the remaining molecules form aggregates that are physisorbed on the early chemisorbed layers [23]. The granular particles (S1) are mostly demonstrating the composition of the cylinder itself. The possible presence of the lubricant components cannot however be excluded. On the cube, EDS analysis in S3 shows a quasi-absence of F detection as compared to C in the 3rd body. It also shows high detection of Zn and Zr, while Zr detection is higher than Zn detection in S4. Consequently, the 3rd body is most likely a combination of components coming from the cube, the cylinder, and the alkyl-phosphonic acid molecules. Both spectrum S2 and S3 demonstrate a very high level of detection of O as compared to Al. Such detection was only observed on ejected debris from

the unlubricated test (Figure 8(b), spectrum S2)). However, in the latter case, F was still detected. Considering the relatively high level of C detection with and without P clear detection, the tribochemical transformation of the molecules remains unclear.

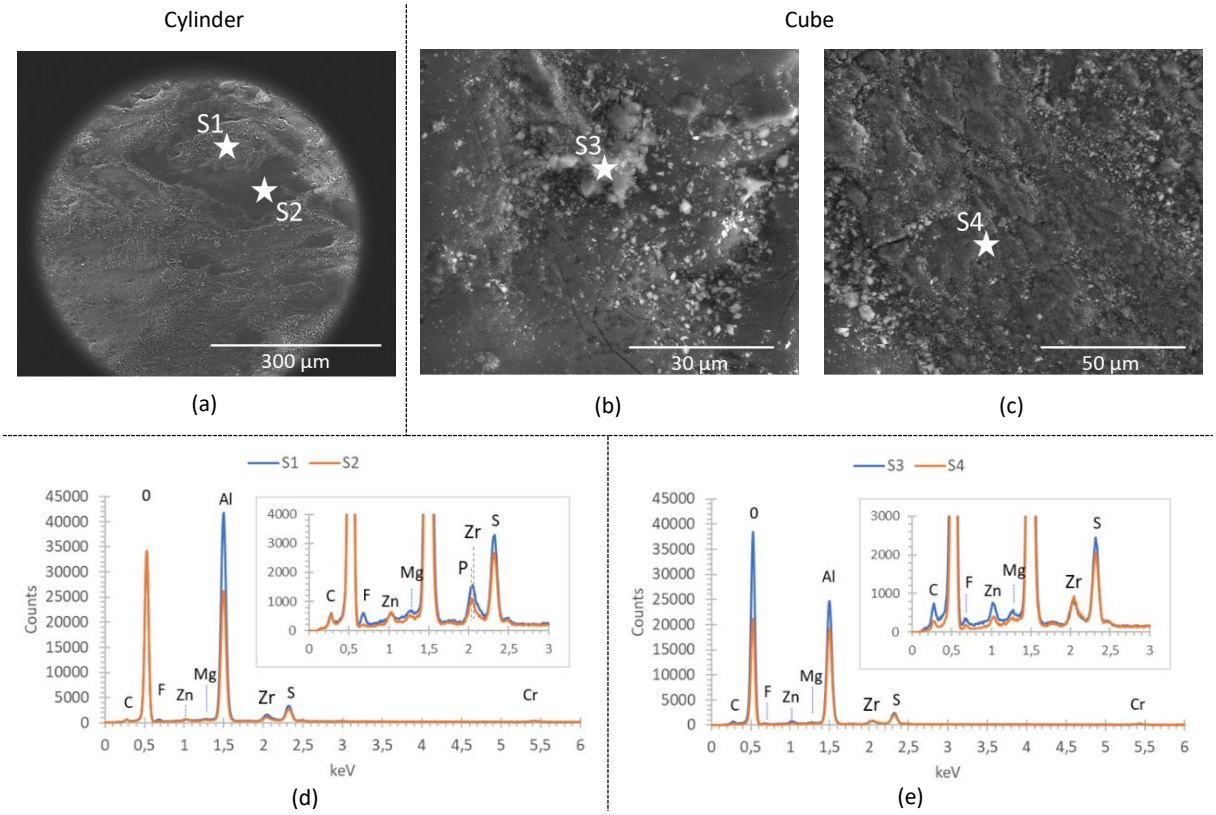


*Figure 14 - SEM images of the thick 3rd body on the cylinder (a), and of the white (b) and dark (c) 3rd bodies on the cube; (d) and (e) are the EDS spectra of 3rd bodies from both the cylinder and the cube respectively. Samples from the tests lubricated with alkyl-phosphonic acid molecules*

FTIR measurements have hence been conducted on the 3rd body and compared with the pristine molecules in their different forms: as crystals before they are dispersed and dissolved in the solvent, as agglomerates which forms during solvent evaporation, and as self-assembled layer (SAM). The three sharp bands close to 2920, 2850, and 1450 cm-1 on the spectra and associated to the pristine molecules (Figures 13c and 13d) are attributed to C-H antisymmetric stretching, C-H symmetric stretching, and C-CH2 scissors vibration modes, respectively [21]. They correspond to the vibration modes related to the presence of alkyl chains. Further multiple peaks appearing in the 1200–900 $cm^{-1}$ region are attributed to chemical bonds containing phosphorus such as P-O-C stretching (1055-915 $cm^{-1}$) and P=O stretching (1200 $cm^{-1}$) [24]. Note that the low absorption signal collected only at 2920 and 2850 $cm^{-1}$ in the case of the SAM layer is consistent with its thinness on the substrate as compared to the penetration depth of analysis that exceeds a few micrometer [25]. The overall ATR-FTIR spectrum shape is significantly modified when analyses are performed on the 3rd bodies (Figure 13a and 13b). Such modification indicates that the molecules underwent significant tribologically induced transformations. In the case of the 3rd body on the cube sample, the strong and broadband absorption signal at 1100 $cm^{-1}$, and in the 3600-3100 $cm^{-1}$ region could be assigned to C-O stretching and C-O-H stretching, respectively. The peaks at 2920 and 2850 $cm^{-1}$ are also dramatically reduced. These results suggest that alkyl chains have been partially degraded, and that they have most likely reacted with substrate oxides during friction to form new compounds. The 3rd body is comprised of those new compounds. Moreover, bonds related to phosphorus products are no longer observed on the spectrum while low absorption appears in the 1350-1500 $cm^{-1}$ and 1500-1700 $cm^{-1}$ regions. The first absorption region could result from the presence

of C-OO symmetric stretching [24]. The second absorption region might be assigned to both C=C and C=O bonds. Most interestingly, the spectrum in this region appears similar to those obtained when analyzing graphene oxide material [26–28]. Such transformation of the molecules into graphene oxide like material may explain why the remaining adhesion measured during the opening of the contact, after unloading, is so low. Amorphous carbon and graphene based lubricious interface were indeed observed upon tribochemical reactions in contacts lubricated with methane [29], isopropyl alcohol [30], and ethylene glycol [31]. Moreover, graphene oxide has already demonstrated lubricious capabilities in macroscale contacts [32]. The very weak signal collected on the 3rd body of the cylinder is most likely related to its thinness. Nonetheless, the presence of a small band at 1100 cm-1, similar to that observed with the 3rd body on the cube, confirms that significant transformation of the molecules occurred.

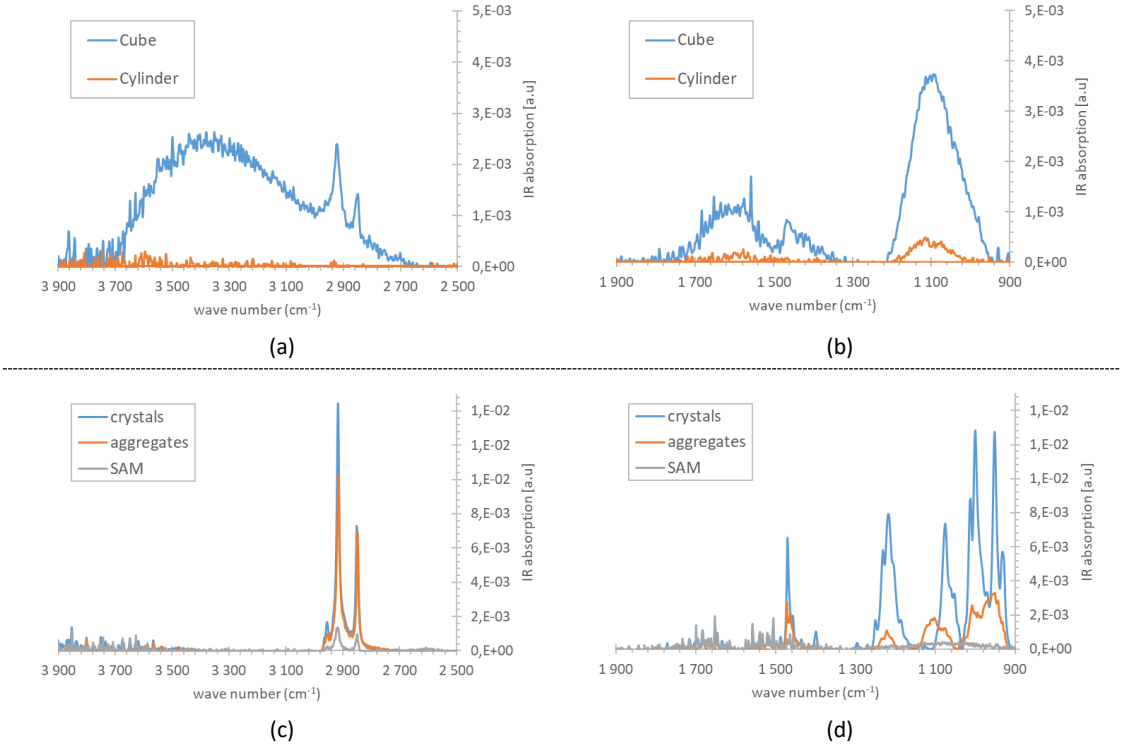


*Figure 15 - FTIR analyses of the 3rd body created from alkyl-phosphonic acid molecules-based lubricants (a, b), and of the pristine alkyl-phosphonic acid molecules in their different forms (c, d)*

# 5 Summary

During preflight qualification tests, a CubSat satellite did not pass the ejection test due to the occurrence of fretting wear between the dispenser's guiding rails and Cubesat's rail counterparts. Considering the development stage of the CubSat, not a single part could be changed and lubrication had to be applied on the damaged parts to insure successful launch.

The study herein hence aimed at (1) understanding the mechanisms driving the fretting wear anomaly, and (2) at testing lubrication solutions to be applied on the damaged parts of the satellite. Based on the expertise of the CubSat and the qualification test data, a tribometer scale study has been designed. The wear morphologies observed on real parts have been reproduced at the tribometer scale. It has been found that the anomaly is indeed due to fretting wear, which leads to the creation of a large amount of debris circulating inside the contact and being ejected outside of it. Debris that are trapped inside the contact agglomerated into large 3rd body patches that created strong adhesive bounds

between the parts. High friction coefficient (0.7) and high normal adhesion force were measured. The main source of wear particles was the satellite materials.

Two lubricants have been tested to provide efficient lubrication at the damaged contacts: a space qualified Perfluoropolyether (PFPE) based grease with Polytetrafluoroethylene (PTFE) particles dispersed in it on one hand, and alkyl-phosphonic acid molecule-based lubricant on the other hand. The grease has been shown to perform the best. All along the fretting test, the friction remained low (0.1) and the normal adhesion force measured at the contact opening has been reduced by ~20%. compared to the unlubricated case. The reason for such behavior are:

1. the creation of a PTFE based 3rd body layer all over the surfaces of sample emulating the dispenser rail with the thickest parts on the initially damaged areas
2. The creation of thick 3rd body layer inside the damaged area of the sample emulating the satellite rail.

The alkyl-phosphonic acid molecules-based lubricant demonstrated similar friction reduction. However, the onset of lubrication failure appeared at half of the fretting tests duration. The successful lubrication of the first half of the test is believed to be due to the creation of a graphene oxide-based lubricious 3rd body layer by tribochemical reaction of the molecules with the substrate materials. However, it appears to either not cover all the contact area leaving some portion of the substrates' surfaces exposed to allow direct contacts between them; or not be stable enough within the contact to sustain such harsh conditions and be ejected outside the contact. Nonetheless, after the adhesive bounds between the substrates are broken and surfaces are only separated by the 3rd body, the remaining adhesion between parts is reduced by 30% as compared to the unlubricated contact case, i.e. lower than with the grease. Such in-situ creation of graphene oxide-like materials from alkyl-phosphonic acid molecules hence remains of great interest and needs further investigations.

The grease lubricant has been applied on the CubSat satellite, which eventually successfully passed the test, and was successfully launched.

# 6 Acknowledgements

This work was financially supported by the French space agency (CNES). The authors wish to thank Xavier Roizard for providing them with alkyl-phosphonic acid solutions, Luc Carpentier for helping to repair the Plint TE77 tribometer.

# 7 References

[1] A. Rivera, A. Stewart, Study of Spacecraft Deployables Failures, in: Proc. 19th Eur. Sp. Mech. Tribol. Symp. - ESMATS 2021, On line, 2021.

[2] A. Merstallinger, R. Holzbauer, N. Bamsey, Cold welding in hold down points of space mechanisms due to fretting when omitting grease, Lubricants. 9 (2021). https://doi.org/10.3390/lubricants9080072.

[3] M. Johnson, The Galileo High Gain Antenna Deployment anomaly, Pasadena, CA, 1989.

[4] ECSS-E-10-03A, Space engineering _ Testing, (2002) 174. https://doi.org/10.1142/9781860944574_0014.

[5] D. Wyn-Roberts, New frontiers for space tribology, Tribol. Int. 23 (1990) 149–155. https://doi.org/10.1016/0301-679X(90)90050-Y.

[6] ECSS-Q-ST-70-01C, Space Product Assurance - Software Product Assurance, (2008) 75.

[7] R.L. Fusaro, Tribology needs for future space and aeronautical systems, 1991.

[8] ECSS-E-ST-32C Rev. 1, Space engineering _ Structural general requirements, (2008) 134.

[9] J.R. Jones, Lubrication, Friction, and Wear NASA/SP-8063, 1971. https://doi.org/10.1002/9781118907948.ch6.

[10] P.L. Conley, Space Vehicle Mechanisms: Elements of Successful Design, John Wiley and Sons, 1998.

[11] R.B. Waterhouse, Fretting wear, Wear. 100 (1984) 107–118. https://doi.org/10.1016/0043-1648(84)90008-5.

[12] Z. Cai, M. Zhu, H. Shen, Z. Zhou, X. Jin, Torsional fretting wear behaviour of 7075 aluminium alloy in various relative humidity environments, Wear. 267 (2009) 330–339. https://doi.org/10.1016/j.wear.2009.01.024.

[13] Z.R. Zhou, S. Fayeulle, L. Vincent, Cracking behaviour of various aluminium alloys during fretting wear, Wear. 155 (1992) 317–330. https://doi.org/10.1016/0043-1648(92)90091-L.

[14] M. Varenberg, G. Halperin, I. Etsion, Different aspects of the role of wear debris in fretting wear, Wear. 252 (2002) 902–910. https://doi.org/10.1016/S0043-1648(02)00044-3.

[15] Y.K. Chen, L. Han, A. Chrysanthou, J.M. O'Sullivan, Fretting wear in self-piercing riveted aluminium alloy sheet, Wear. 255 (2003) 1463–1470. https://doi.org/10.1016/S0043-1648(03)00274-6.

[16] K. Elleuch, S. Fouvry, Wear analysis of A357 aluminium alloy under fretting, Wear. 253 (2002) 662–672. https://doi.org/10.1016/S0043-1648(02)00116-3.

[17] Z.R. Zhou, Q.Y. Liu, M.H. Zhu, L. Tanjala, P. Kapsa, L. Vincent, Investigation of fretting behaviour of several metallic materials under grease lubrication, Tribol. Int. 33 (2000) 69–74. https://doi.org/10.1016/S0301-679X(99)00100-0.

[18] N. Arun Prakash, R. Gnanamoorthy, M. Kamaraj, Fretting wear behavior of controlled ball impact treated aluminium alloy under dry sliding condition, Surf. Coatings Technol. 207 (2012) 450–460. https://doi.org/10.1016/j.surfcoat.2012.07.045.

[19] J. Qi, J. Światowska, P. Skeldon, P. Marcus, Chromium valence change in trivalent chromium conversion coatings on aluminium deposited under applied potentials, Corros. Sci. 167 (2020). https://doi.org/10.1016/j.corsci.2020.108482.

[20] B. Greene, NASA and ESA Collaboration on Hexavalent Chrome Free Coatings, in: Int. Work. Environ. Altern. ENERGY, Noordwijk, The Netherleands, 2017: pp. 1–23.

[21] P.H. Cornuault, J.M. Melot, X. Roizard, F. Lallemand, Dry lubrication of ferritic stainless steel functionalised with crystalline aggregates of hexadecylphosphonic acid, Tribol. Int. 145 (2020) 106139. https://doi.org/10.1016/j.triboint.2019.106139.

[22] P. Zhang, L. Zeng, X. Mi, Y. Lu, S. Luo, W. Zhai, Comparative study on the fretting wear property of 7075 aluminum alloys under lubricated and dry conditions, Wear. 474–475 (2021) 203760. https://doi.org/10.1016/j.wear.2021.203760.

[23] W. Gao, L. Dickinson, C. Grozinger, F.G. Morin, L. Reven, Self-assembled monolayers of alkylphosphonic acids on metal oxides, Langmuir. 12 (1996) 6429–6435. https://doi.org/10.1021/la9607621.

[24] J.B. Lambert, H.F. Shurvell, D.A. Lightner, R.G. Cooks, Introduction to organic spectroscopy, Macmillan Publishing Company, 1987.

[25] K.L.A. Chan, S.G. Kazarian, Attenuated total reflection fourier transform infrared imaging with variable angles of incidence: A three-dimensional profiling of heterogeneous materials, Appl. Spectrosc. 61 (2007) 48–54. https://doi.org/10.1366/000370207779701415.

[26] Y. Gao, L.Q. Liu, S.Z. Zu, K. Peng, D. Zhou, B.H. Han, Z. Zhang, The effect of interlayer adhesion on the mechanical behaviors of macroscopic graphene oxide papers, ACS Nano. 5 (2011) 2134–2141. https://doi.org/10.1021/nn103331x.

[27] P.M. Sudeep, T.N. Narayanan, A. Ganesan, M.M. Shaijumon, H. Yang, S. Ozden, P.K. Patra, M. Pasquali, R. Vajtai, S. Ganguli, A.K. Roy, M.R. Anantharaman, P.M. Ajayan, Covalently Interconnected Three Dimensional Graphene Oxide Solids., ACS Nano. (2013) 7034–7040. https://doi.org/10.1021/nn402272u.

[28] M. Acik, C. Mattevi, C. Gong, G. Lee, K. Cho, M. Chhowalla, Y.J. Chabal, <The Role of Intercalated Water in Multilayered Graphene Oxide_ACSNano2010_Ceci_Water Supporting Info.pdf>, 4 (2010) 5861–5868.

[29] G. Ramirez, O.L. Eryilmaz, G. Fatti, M.C. Righi, J. Wen, A. Erdemir, Tribochemical Conversion of Methane to Graphene and Other Carbon Nanostructures: Implications for Friction and Wear, ACS Appl. Nano Mater. 3 (2020) 8060–8067. https://doi.org/10.1021/acsanm.0c01527.

[30] R. Zhang, X. Yang, J. Pu, Z. He, L. Xiong, Extraordinary macroscale lubricity of sonication-assisted fabrication of MoS2 nano-ball and investigation of in situ formation mechanism of graphene induced by tribochemical reactions, Appl. Surf. Sci. 510 (2020) 145456. https://doi.org/10.1016/j.apsusc.2020.145456.

[31] R. Zhang, Q. Chen, Z. He, L. Xiong, In situ friction-induced amorphous carbon or graphene at sliding interfaces: Effect of loads, Appl. Surf. Sci. 534 (2020) 146990. https://doi.org/10.1016/j.apsusc.2020.146990.

[32] L. Chen, G. Wu, Y. Huang, C. Bai, Y. Yu, J. Zhang, High Loading Capacity and Wear Resistance of Graphene Oxide/Organic Molecule Assembled Multilayer Film, Front. Chem. 9 (2021) 1–9. https://doi.org/10.3389/fchem.2021.740140.